Chem

CellPress

Article

Ladder-type conjugated molecules as robust multi-state single-molecule switches

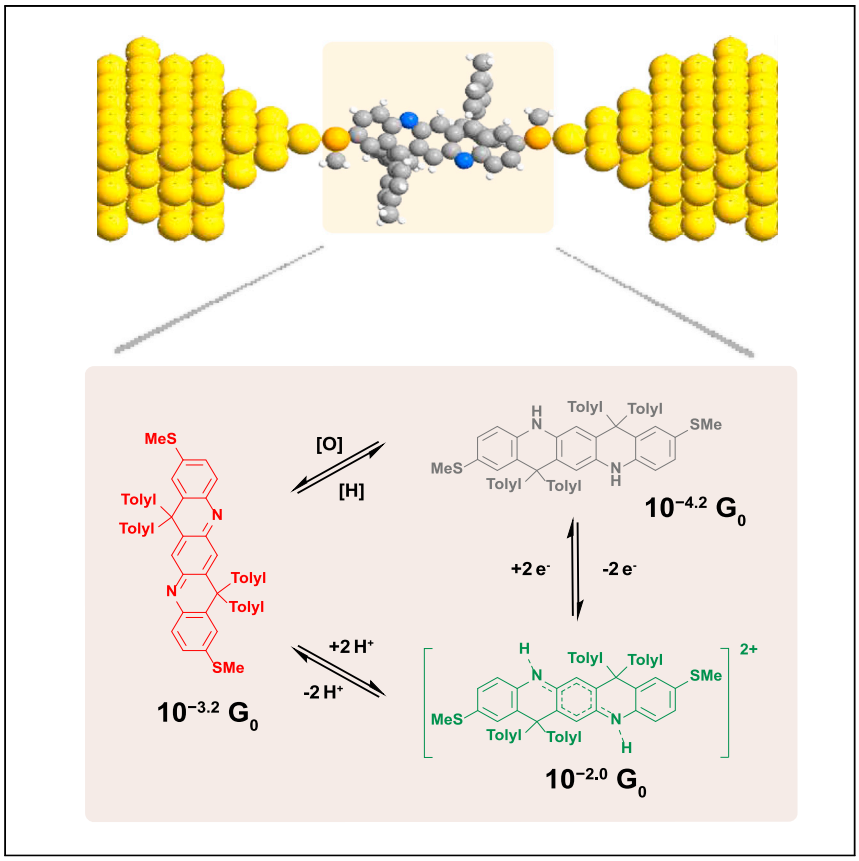

Fusing the molecular structure of an oligoaniline derivative into a ladder-type constitution stabilizes its redox and protonation states. The ladder-type molecule exhibits robust and reversible switching of single-molecule conductance among three different states, with the protonated and oxidized state exhibiting the highest conductance. This work advances the mechanistic understanding of the electronic properties of conductive polymers and provides a promising class of organic electronic materials featuring remarkable switchability and stability.

Jialing Li, Bo-Ji Peng, Shi Li, Daniel P. Tabor, Lei Fang, Charles M. Schroeder

fang@chem.tamu.edu (L.F.)
cms@illinois.edu (C.M.S.)

Highlights

Synthesis of a methylthio-functionalized, ladder-type oligoaniline derivative

Excellent stability and high molecular conductance in oxidized and protonated states

Robust switching of single-molecule conductance among three different states

Li et al., Chem 9, 1–16
August 10, 2023
https://doi.org/10.1016/j.chempr.2023.05.001

Please cite this article in press as: Li et al., Ladder-type conjugated molecules as robust multi-state single-molecule switches, Chem (2023), https://doi.org/10.1016/j.chempr.2023.05.001

Chem

CellPress

Article

Ladder-type conjugated molecules as robust multi-state single-molecule switches

Jialing Li,[1,2,3,8] Bo-Ji Peng,[4,8] Shi Li,[4] Daniel P. Tabor,[4] Lei Fang,[4,5,*] and Charles M. Schroeder[1,2,3,6,7,9,*]

SUMMARY

Ladder-type molecular structures greatly enhance the chemical stability of oligoaniline derivatives and impart well-defined physical properties to multiple molecular charge states. In this work, we characterize the charge transport properties of a ladder-type cyclohexadiene-1,4-diimine derivative at various protonation, lithiation, and oxidation states using single-molecule techniques. Our results show that a ladder-type oligoaniline derivative serves as a robust and reversible molecular switch with over two orders of magnitude changes in molecular conductance when controlled using chemical or electrochemical stimuli. Experimental results are complemented by molecular modeling using density functional theory (DFT) and nonequilibrium Green's function-DFT (NEGF-DFT) to elucidate charge transport mechanisms at different molecular states. Overall, this work provides new strategies for advancing the stability, programmability, and efficiency of molecular charge transport using ladder-type single-molecule switches.

INTRODUCTION

Recent advances in molecular electronics have been fueled by the development of new chemistries and an improved understanding of charge transport mechanisms.[1–4] Single-molecule electronic devices are commonly fabricated as junctions consisting of a central molecular bridge containing two terminal anchor groups connected to metal electrodes. Efficient and stable charge transport critically relies on the anchor-electrode combination and the overall molecular design. Single-molecule devices with programmable functionality have been created by incorporating stimuli-responsive chemical moieties into the molecular bridge.[5] Using this approach, efficient switching of electric signals at the single-molecule level has been achieved using a wide array of external stimuli such as pH,[6] optical fields,[7] electric fields,[8] magnetic fields,[9] mechanical forces,[10] and electrochemical control.[11,12] By leveraging advances in stimuli-response electronics, single-molecule organic electrochemical transistors (OECTs) have recently been developed.[13]

Bulk OECT devices have been extensively used in biosensing and bioelectronics applications including metabolite sensing,[14] ion sensing,[15] electrophysiological sensors,[16] and neuromorphic computing.[17] High degrees of electrochemical stability are critically required for robust and active OECT materials.[18,19] In general, OECT materials should be capable of adopting two or more states showing significant differences in molecular conductance that can be controlled using redox chemistry or ion-binding processes.[20] Despite recent progress, achieving multi-state stimuli responses in functional organic materials remains challenging due to complexities in molecular design, synthesis, and poor stability of many organic molecules through multiple switching cycles.[19,21,22]

THE BIGGER PICTURE

Achieving a fundamental understanding of materials for molecular electronics is essential for advancing the cutting-edge fields of neuromorphic computing, artificial intelligence, and human-computer interaction. Acquiring insight into molecular charge transport mechanisms and elucidating their modulation in response to chemical transformations are crucial for guiding the design of functional organic materials such as electronically switchable molecules. In this work, we study the molecular conductance of a highly robust, multi-state molecular switch featuring a ladder-type oligoaniline structure, which shows stable and reversible switching of conductance over two orders of magnitude through chemical or *in situ* electrochemical control. Experiments are supported by computational modeling, which sheds light on the mechanism of these conductance states. This research demonstrates that robust ladder-type redox-active molecules are highly promising for molecular electronics applications.

Please cite this article in press as: Li et al., Ladder-type conjugated molecules as robust multi-state single-molecule switches, Chem (2023), https://doi.org/10.1016/j.chempr.2023.05.001

Polyaniline (PANI) is a promising organic material for molecular electronics due to its versatile chemical and electrochemical doping properties that enable access to multiple charge states. Although the conjugation pattern and conductivity along the PANI backbone can be modulated into different states,[23] PANI suffers from chemical instabilities in acidic or oxidative environments.[24] In addition, the functional aniline core contains single C–N bonds connecting adjacent aromatic rings, allowing for facile backbone rotation that inhibits control over charge transport efficiency.[25] In general, the charge transport efficiency in linear conjugated molecules critically depends on the dihedral angles between adjacent conjugated units.[26] In linear conjugated backbones, dihedral angles are controlled by the chemical identity of substituted side chains,[27] molecular lengths,[28] temperatures,[29] electric fields,[30] and the solvation environment.[31] Implementing a ladder-type constitution in conjugated molecules provides an effective strategy to restrict the molecular backbone rotation while further enhancing the chemical and mechanical stabilities of conjugated molecules.

Ladder-type structures can be used to enhance the electronic properties of conjugated molecules by imparting molecular-scale control over backbone rotation and enforcing a desired coplanar conformation.[32] The resulting rigid coplanar ladder-type molecules allow for intramolecular charge transport with coherent electron delocalization, which mitigates the length-dependent decay in molecular conductance.[32–34] The rigid coplanar conformation further enhances intermolecular coupling due to the reduced reorganization energy upon charge transfer.[35] Prior work has reported that the ladder-type constitution imparts high levels of stability into the protonated and oxidized states of PANI derivatives by preventing hydrolysis and isomerization, thereby enabling fundamental studies of charge transport in ladder-type molecules.[24,36] From this view, ladder-type conjugated molecules allow for stable chemical states that give rise to significantly different molecular conductance levels under ambient conditions and provide access to multi-state switching at the single-molecule level.

In this work, we study the charge transport properties of ladder-type aniline derivatives using single-molecule techniques. We hypothesized that the ladder-type constitution would provide robust stability allowing for controlled chemical and electrochemical manipulation of molecular conductance. To validate this hypothesis, we synthesized a methylthio-functionalized, ladder-type cyclohexadiene-1,4-diimine-derivative that is analogous to oligoaniline. Our results show that the ladder-type cyclohexadiene-1,4-diimine-derivative exhibits robust multi-state conductance switching in single-molecule junctions using chemical and electrochemical stimuli. In particular, the conjugated ladder-type pernigraniline-based molecule **TolMSQ** can be switched from a neutral quinoidal to a positively charged species where the quinoidal $[\mathbf{TolMSQ\text{-}2H}]^{2+}$ and benzenoidal $[\mathbf{TolMSQ\text{-}2H}]^{2+\bullet}$ structures are in resonance (Scheme 1). Our results show that the quinoidal structure **TolMSQ** promotes efficient molecular charge transport, whereas the fully protonated $[\mathbf{TolMSQ\text{-}2H}]^{2+}$ or lithiated $[\mathbf{TolMSQ\text{-}2Li}]^{2+}$ states possess an air stable diradical open-shell resonance that further enhances molecular conductance beyond the quinoidal state. Electrochemical potential is further varied to reversibly switch molecular conductance between states with an on/off ratio of over 100 on a single-molecule device. Density functional theory (DFT) calculations reveal higher orbital weights on terminal anchor groups in the fully conjugated neutral and charged states with a corresponding decrease in energy gaps compared with the neutral benzenoidal state, consistent with single-molecule conductance experiments. Overall, this work shows that ladder-type conjugated molecules are promising materials for molecular electronic devices with remarkable switching behavior.

[1]Department of Chemical and Biomolecular Engineering, University of Illinois at Urbana-Champaign, Urbana, IL 61801, USA

[2]Beckman Institute for Advanced Science and Technology, University of Illinois at Urbana-Champaign, Urbana, IL 61801, USA

[3]Joint Center for Energy Storage Research, Argonne National Laboratory, 9700 South Cass Avenue, Lemont, IL 60439, USA

[4]Department of Chemistry, Texas A&M University, College Station, TX 77843, USA

[5]Department of Material Science and Engineering, Texas A&M University, College Station, TX 77843, USA

[6]Department of Materials Science and Engineering, University of Illinois at Urbana-Champaign, Urbana, IL 61801, USA

[7]Department of Chemistry, University of Illinois at Urbana-Champaign, Urbana, IL 61801, USA

[8]These authors contributed equally

[9]Lead contact

*Correspondence: fang@chem.tamu.edu (L.F.), cms@illinois.edu (C.M.S.)

https://doi.org/10.1016/j.chempr.2023.05.001

Please cite this article in press as: Li et al., Ladder-type conjugated molecules as robust multi-state single-molecule switches, Chem (2023), https://doi.org/10.1016/j.chempr.2023.05.001

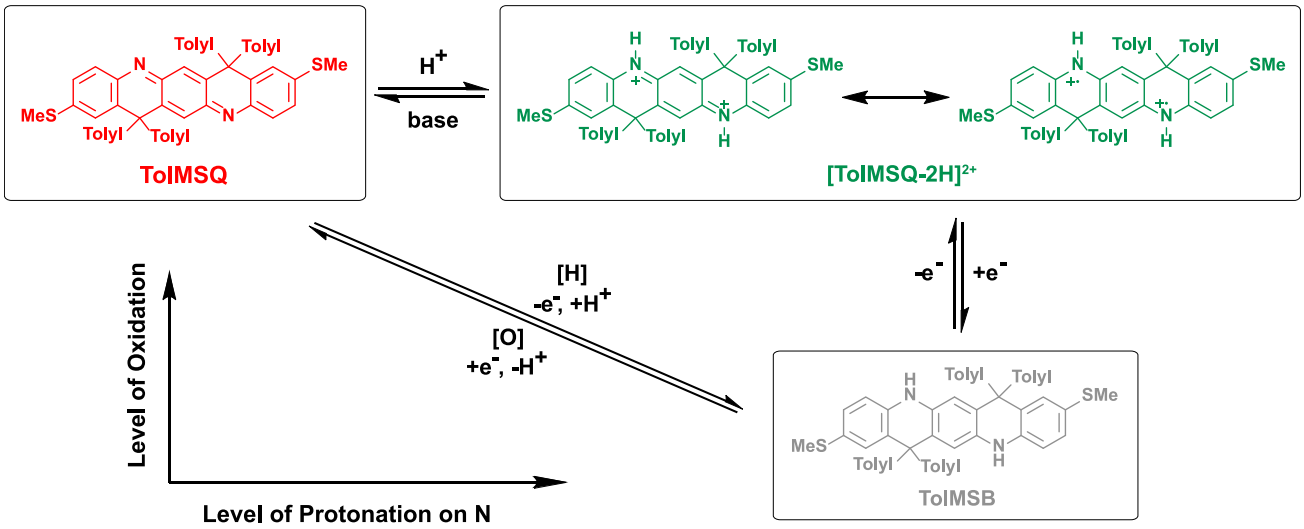

Scheme 1. Multi-state molecular transformation routes of the fully conjugated ladder-type TolMSQ molecule

RESULTS AND DISCUSSION

Design and synthesis

TolMSQ was synthesized by preparing a *p*-phenylenediamine-centered derivative **4** through imine condensation between 4-(methylthio)aniline **1** and dimethylsuccinyl succinate **2** (Scheme 2). During the reaction, the enamine intermediate **3** precipitated due to its limited solubility. An oxidation step was used on a dispersed suspension of **3** in a mixture of THF (tetrahydrofuran)/$CHCl_3$ (1:1 volume) under reflux conditions to convert **3** to the oxidized form **4**. Subsequently, **4** was subjected to a 4-fold Grignard reaction with *p*-tolyl magnesium bromide, followed by an acid-catalyzed Friedel-Crafts ring cyclization. The resulting fused-ring benzenoid product TolMSB is a small molecule analog of leucoemeraldine, which is the reduced form of PANI. TolMSB was further oxidized by Ag_2O with ultrasonication in small batches to afford the quinonoid compound TolMSQ, which represents a small molecule analog of pernigraniline base. The structure of TolMSQ was fully characterized by NMR and high-resolution mass spectrometry (Figures S1–S4).

Single-molecule charge transport in multiple molecular states

A reversible transformation between the quinoidal TolMSQ and benzenoidal TolMSB can be achieved via simple addition of chemical reagents, resulting in drastic changes in electronic properties.[37,38] Our results show that the benzenoid TolMSB is readily accessed by chemically reducing 0.05 mM TolMSQ with the addition of 10 equiv *N*,*N*-diethylhydroxylamine (DEHA) in 1,2,4-trichlorobenzene (TCB) solution (Figure 1A). TolMSB remained stable in ambient conditions for days. The quantitative conversion from TolMSQ to TolMSB was validated by mass spectrometry and solution-state ^{1}H NMR (Figure S5). UV-vis absorption spectra also confirmed the chemical reduction of TolMSQ (Figure 1B). Upon addition of DEHA, the characteristic charge-transfer band centered around 520 nm was no longer observed, which indicates the transformation from a fully conjugated backbone (TolMSQ) to a non-conjugated backbone (TolMSB).

We next characterized the charge transport properties of TolMSQ and TolMSB using single-molecule experiments. Molecular charge transport was characterized using the scanning tunneling microscope-break junction (STM-BJ) technique, as

Please cite this article in press as: Li et al., Ladder-type conjugated molecules as robust multi-state single-molecule switches, Chem (2023), https://doi.org/10.1016/j.chempr.2023.05.001

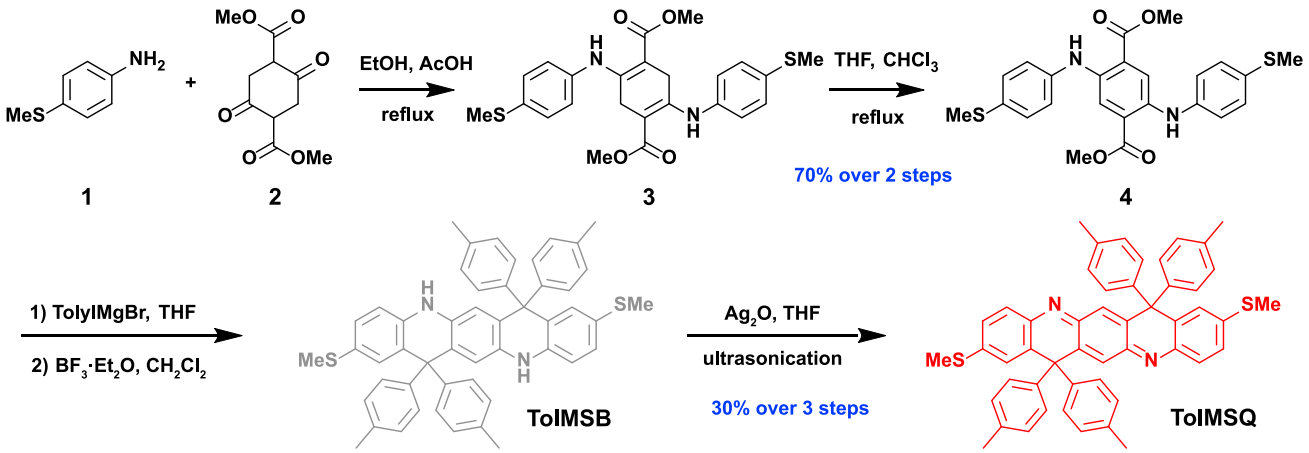

Scheme 2. Synthesis of TolMSQ

described in our prior work (supplemental information).[39–41] In each experiment, molecular conductance versus displacement measurements are obtained from 7,000 to 10,000 individual molecular junctions formed between a gold tip and substrate electrode. The resulting traces are compiled without data selection into a one-dimensional (1D) logarithmically binned histogram fit with a Lorentzian function, where the peak value is determined as the most probable conductance of the molecular junction. Figure 1C shows that the quinoidal **TolMSQ** molecule exhibits a conductance peak around $10^{-3.2}$ G_0, where G_0 is the conductance quantum $2e^2/h$ (where e is the electron charge and h is Planck's constant). In contrast, the reduced benzenoidal **TolMSB** species shows an average molecular conductance of $10^{-4.2}$ G_0, which is approximately 10 times smaller than that of **TolMSQ**.

Two-dimensional (2D) conductance versus displacement histograms are further constructed by compiling all molecular trajectories in each experiment (Figures 1C and 1D). Based on the 2D histograms, **TolMSQ** displays a slightly longer and less steep conductance plateau compared with **TolMSB** due to a more rigid backbone from the quinoidal character. Junction displacements of **TolMSQ** were further analyzed by 1D displacement histograms as previously described (Figure S6).[40] Our results show that the average length of **TolMSQ** junctions is approximately 1.3 nm (after accounting for snap-back distance arising from atomic rearrangements upon gold nanowire rupture),[42] which is consistent with the end-to-end molecular backbone length of **TolMSQ** from DFT calculations (Table S4) (*vide infra*). This molecular junction length excludes the possibility of alternative conductance pathways through the internal nitrogen atoms. Prior work reported that a non-ladder oligoaniline-derived molecule presents multiple conducting pathways induced by an electric field, which leads to poorly controlled electronic properties due to structural flexibility.[43] The ladder-type **TolMSQ** molecule overcomes these challenges, showing stable conductance values over a wide range of applied biases with a well-defined conductance peak (Figure S7).

We next showed that the conductance of **TolMSQ** in single-molecule junctions can be reversibly switched between the neutral and protonated states by addition of Brønsted acids and bases (Figure 2). Unlike conventional non-ladder type oligoaniline or PANI molecules that are readily degraded in acidic conditions,[24,44,45] the ladder-type constitution significantly enhances the stability, and a clear transition is

Please cite this article in press as: Li et al., Ladder-type conjugated molecules as robust multi-state single-molecule switches, Chem (2023), https://doi.org/10.1016/j.chempr.2023.05.001

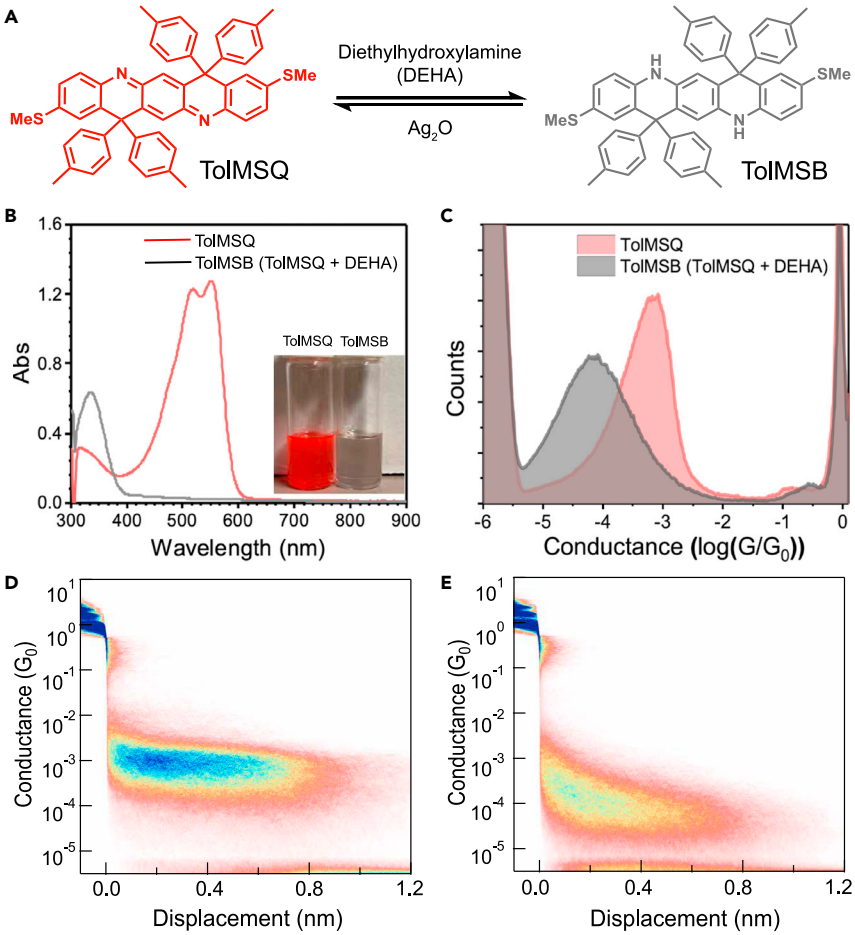

Figure 1. Reversible transformation between TolMSQ and TolMSB and single-molecule conductance experiments

(A) Chemical transformation between the two states using reducing and oxidizing reagents.

(B) UV-vis absorption spectra for **TolMSQ** (0.05 mM in TCB, red) and **TolMSB** (0.05 mM, gray) after adding 10 equiv DEHA to the **TolMSQ** solution; inset: photographic images of **TolMSQ** and **TolMSB** solutions.

(C) 1D conductance histograms of 0.05 mM **TolMSQ** (red) and **TolMSB** (gray) in TCB solution. All 1D conductance histograms are compiled from 7,000 individual single molecule measurements and normalized by the total number of measurements without data selection.

(D and E) 2D conductance versus displacement histograms of 0.05 mM **TolMSQ** and **TolMSB** in TCB solution, respectively, at 250 mV applied bias constructed from 7,000 individual traces without data selection.

observed between two protonation stages in UV-vis absorption bands. Upon addition of methanesulfonic acid (MSA) to a 0.05 mM **TolMSQ** solution in TCB, the UV-vis absorption spectra red shfit into the near-infrared (NIR) region, together with an obvious change in solution color (Figures 2B and S8). After protonation, the resulting $[\mathbf{TolMSQ}\text{-}2H]^{2+}$ state is expected to exhibit significantly stronger open-shell diradical character due to the contribution of open-shell 6π Huckel aromatic resonance and open-shell 4π Baird aromatic resonance structures.[46] Indeed, the solution-phase electron paramagnetic resonance (EPR) spectroscopy spectra of TolMSQ in the presence of 0.1 M trifluoroacetic acid (TFA) shows a strong EPR signal (*g* factor = 2.0021), whereas the neutral form of **TolMSQ** exhibits no detectable EPR signal at room temperature (Figure 2C).

Please cite this article in press as: Li et al., Ladder-type conjugated molecules as robust multi-state single-molecule switches, Chem (2023), https://doi.org/10.1016/j.chempr.2023.05.001

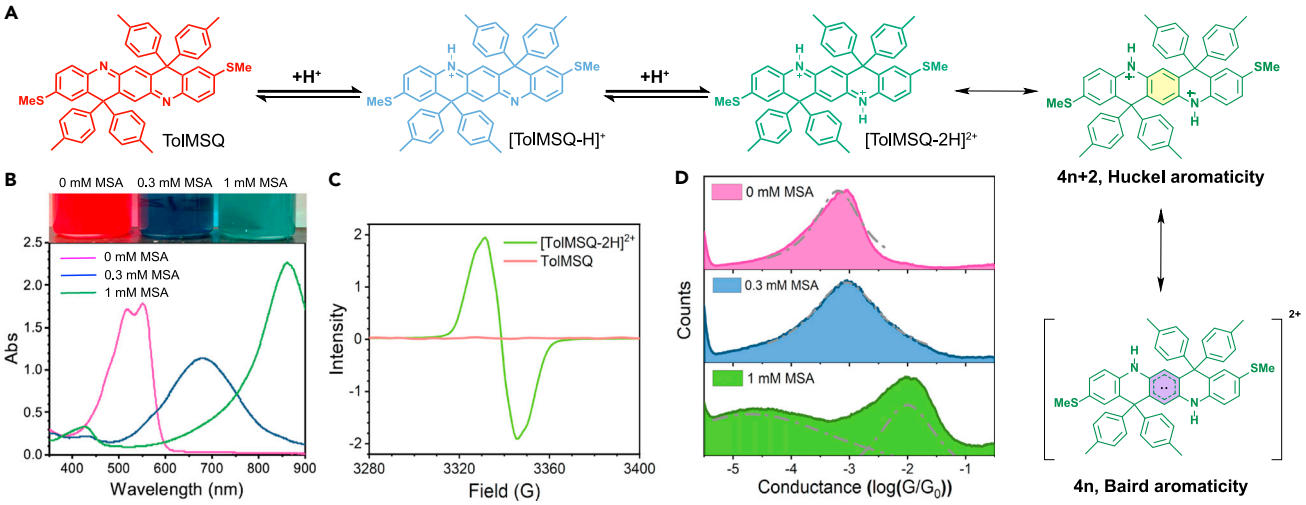

Figure 2. Reversible switching of molecular conductance in TolMSQ

(A) The protonation process of **TolMSQ** to [**TolMSQ-H**]$^{+}$ and [**TolMSQ-2H**]$^{2+}$.

(B) (Top) Photographic images and (bottom) UV-vis absorption spectra corresponding to the three stages of protonation of **TolMSQ** (0.05 mM in TCB).

(C) EPR spectra of [**TolMSQ-2H**]$^{2+}$ (green, *g* value = 2.0021, 1.0 mM in CH_2Cl_2 with 1 M MSA) and **TolMSQ** (red, 10 mM in CH_2Cl_2/TEA = 10/1).

(D) 1D conductance histograms of unprotonated **TolMSQ** (top), [**TolMSQ-H**]$^{+}$(middle), and [**TolMSQ-2H**]$^{2+}$ (bottom) measured in TCB at 250 mV applied bias. 1D conductance histograms are compiled from 5,000 to 10,000 individual single molecule measurements and normalized by the total number of measurements without data selection.

We next characterized single-molecule conductance of **TolMSQ** at each protonation stage upon addition of 0, 0.3, and 1 mM MSA, respectively (Figure 2D). Our results show that the molecular conductance of **TolMSQ** significantly increases at higher protonation states. At an average 50% protonation state, the average molecular conductance of [**TolMSQ-H**]$^{+}$ junctions increases modestly from $10^{-3.2}$ to $10^{-3.0}$ G_0. However, after the second protonation step, the molecular conductance of [**TolMSQ-2H**]$^{2+}$ significantly increases by a factor of 15× compared with **TolMSQ** to $10^{-2.0}$ G_0. Spectral clustering classification was used to further analyze charge transport in molecular junctions, as previously reported,[47,48] which generally confirms that the charge transport was measured from end-to-end junction connections in all cases (Figures S9–S11; Tables S1–S3). These results support our hypothesis that the protonated oxidized form of aniline derivatives, such as the pernigraniline salt form of PANI, are highly conductive. These findings are also consistent with our prior experiments on the bulk conductivity and Pauli paramagnetism of ladder-type pernigraniline salts after acid doping.[24,36]

Interestingly, our results show an unexpected second peak in the 1D conductance histogram of [**TolMSQ-2H**]$^{2+}$ (Figure 2D). To further investigate the origins of the low conductance (low *G*) peak, we first assessed the reversibility of acid doping to characterize the structural integrity during the chemical transformation. In these experiments, UV-vis absorption spectra and molecular conductance measurements were obtained after the sequential addition of 2 mM MSA, followed by 2 mM triethylamine (Et_3N), to a 0.05 mM **TolMSQ** solution (Figure S12). UV-vis absorption data show that the intensity of the absorption peak remains the same before and after the acid-base addition without material loss, whereas the low *G* peak disappears upon the addition of Et_3N (Figure S13). These results suggest that the low *G* peak does not arise due to degradation of the protonated species. We hypothesized that multiple conductance states (high *G* and low *G*) arise either due to multiple charge transport pathways arising from intramolecular transport through a single

Please cite this article in press as: Li et al., Ladder-type conjugated molecules as robust multi-state single-molecule switches, Chem (2023), https://doi.org/10.1016/j.chempr.2023.05.001

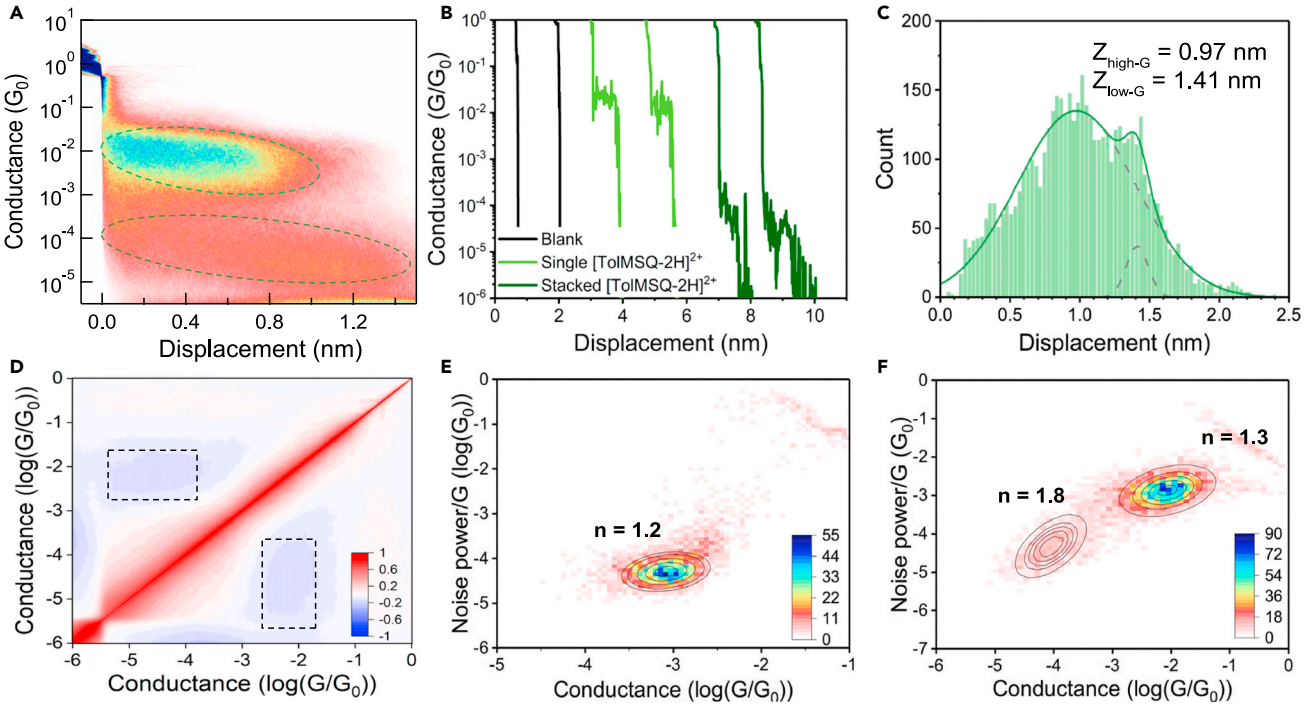

Figure 3. Single-molecule conductance of TolMSQ and different charge states

(A) 2D conductance-versus-displacement histogram of **[TolMSQ-2H]$^{2+}$** measured in TCB solution.

(B) Characteristic individual conductance-displacement traces from break-junction measurement: blank solution (black), junction with high-G (blue), and junction with low-G (green).

(C) 1D displacement histogram of **[TolMSQ-2H]$^{2+}$** without data selection.

(D) 2D correlation analysis of two peaks in the **[TolMSQ-2H]$^{2+}$** measurement.

(E and F) 2D histograms of flicker noise power versus average conductance of **TolMSQ** and **[TolMSQ-2H]$^{2+}$**, respectively. The black ellipses are plotted using results from two-dimensional Gaussian fitting.

[TolMSQ-2H]$^{2+}$ junction or due to intermolecular transport through a stacked **[TolMSQ-2H]$^{2+}$** junction. To understand the molecular origins of the low *G* peak, we first compared the 2D conductance versus displacement histograms of **TolMSQ** at three protonation states (Figures 3A and S14) and examined characteristic single-molecule conductance traces from these conditions (Figure 3B). Characteristic single-molecule traces suggest that junction lengths are within a consistent range among **TolMSQ**, **[TolMSQ-H]$^{+}$**, and the high *G* state of **[TolMSQ-2H]$^{2+}$**, indicating intramolecular transport through a single-molecule junction.

To further understand charge transport pathways in the protonated species **[TolMSQ-2H]$^{2+}$**, we quantified molecular junction displacements during STM-BJ experiments (Figure 3C). Molecular junctions with high conductance values show an average displacement of around ≈1.0 nm, which is consistent with the unprotonated and 50% protonated states. In contrast, the low *G* plateau shows a well-defined longer junction length of around ≈1.4 nm, which indicates the formation of a stacked junction configuration. In addition, concentration-dependent measurements[49] show that the low conductance peak becomes more prominent at higher concentrations (Figure S15), indicating that this peak is likely a result of intermolecular transport. We next analyzed the correlation between the high *G* and low *G* conductance traces using a 2D correlation histogram (Figure 3D).[50,51] 2D correlation histograms plot the normalized covariance matrix from the measured traces, revealing the strength of correlation between pairs of bins in the molecular

Please cite this article in press as: Li et al., Ladder-type conjugated molecules as robust multi-state single-molecule switches, Chem (2023), https://doi.org/10.1016/j.chempr.2023.05.001

conductance histogram. A negative correlation value suggests that the variations of counts in two bins are anti-correlated.[52] Our results show that the high *G* and low *G* peak regions are anti-correlated (Figure 3D), which suggests that the high *G* and low *G* features do not occur in the same individual single-molecule conductance traces and therefore arise from different molecular sub-populations.

Charge transport pathways through a single junction or a stacked dimer junction for **[TolMSQ-2H]$^{2+}$** can be distinguished by the molecular conductance features of through-bond or through-space coupling. The formation of a stacked dimer junction is often dominated by non-covalent intermolecular interactions and subject to fluctuations in the electronic response, which can be quantified by the flicker noise power.[53–55] We performed flicker noise analysis to understand the differences in the transmission pathways of **TolMSQ** (Figure 3E) and two types of junctions from **[TolMSQ-2H]$^{2+}$** (Figure 3F). Unlike the standard STM-BJ pulling-mode measurements, fluctuations in molecular conductance are measured by holding the molecular junction at a fixed tip-to-substrate displacement for 150 ms. In this way, the transient conductance response measured during the holding portion of the experiment is analyzed using a discrete Fourier transformation to obtain the noise power spectral density (PSD) (Figure S16). The flicker noise power of each individual trace is calculated by integrating the PSD between 100 and 1,000 Hz. 2D flicker noise histograms are constructed by sampling all data from the selected traces and fitting with 2D Gaussian.[30,56] A scaling factor *n* is determined by normalizing the noise power by the average conductance to the power of *n* (G^n) while minimizing the correlation between the noise power/G^n and the average conductance. A junction with the noise power scaling of n = 1.0 is dominated by through-bond coupling, whereas the noise power scaling of n = 2.0 is governed by through-space coupling.[53] Our results show that the noise power of **TolMSQ** junctions scales as $G^{1.30}$, which suggests that charge transport is dominated by through-bond coupling. The 2D flicker noise-versus-conductance histogram of **[TolMSQ-2H]$^{2+}$** exhibits two distributions with one scaling as $G^{1.20}$ and the second scaling as $G^{1.80}$, corresponding to the two different molecular sub-populations giving rise to the high *G* and low *G* conductance peaks, respectively (Figure S17). These results suggest that high *G* junctions are dominated by through-bond coupling, but the transmission pathway in low *G* junctions is dominated by through-space coupling in the stacked **[TolMSQ-2H]$^{2+}$** junctions.

Due to the lack of torsional defects, the rigid coplanar backbones of fully conjugated ladder-type molecules give rise to efficient intramolecular charge transport and facilitate strong intermolecular coupling by pi-stacking interactions.[32,57–59] We therefore hypothesized that other ionic Lewis acids such as Li^+ could similarly enhance the conductance of **TolMSQ**. To test this hypothesis, we characterized the molecular conductance of lithium-doped **TolMSQ** in a mixed solvent of TCB/THF (Figure 4A). Prior work has shown that Li^+ ions coordinate with the imine-type nitrogen atoms along the **TolMSQ** backbone.[23,36] Our results show a similar two-step enhancement in molecular conductance upon lithiation as observed in the protonation process (Figures 4B, 4C, and S18). We note that the 1D conductance histogram of fully lithiated **[TolMSQ-2Li]$^{2+}$** also shows a prominent low *G* peak, similar to protonated molecules. Control experiments were performed using tetrabutylammonium tetrafluoroborate ($TBABF_4$) as an inert supporting electrolyte to assess the role of the counter anion on charge transport efficiency (Figure S19). Our results show that the low *G* peak occurs in the absence of protons along the backbone, which excludes the possibility of H-bonding promoting dimerization in the presence of lithium. Weak dispersion interactions such as π-π interactions in conjugated systems could give rise to stacking in **[TolMSQ-2H]$^{2+}$** and **[TolMSQ-2Li]$^{2+}$** dimers.[60] In this scenario,

Please cite this article in press as: Li et al., Ladder-type conjugated molecules as robust multi-state single-molecule switches, Chem (2023), https://doi.org/10.1016/j.chempr.2023.05.001

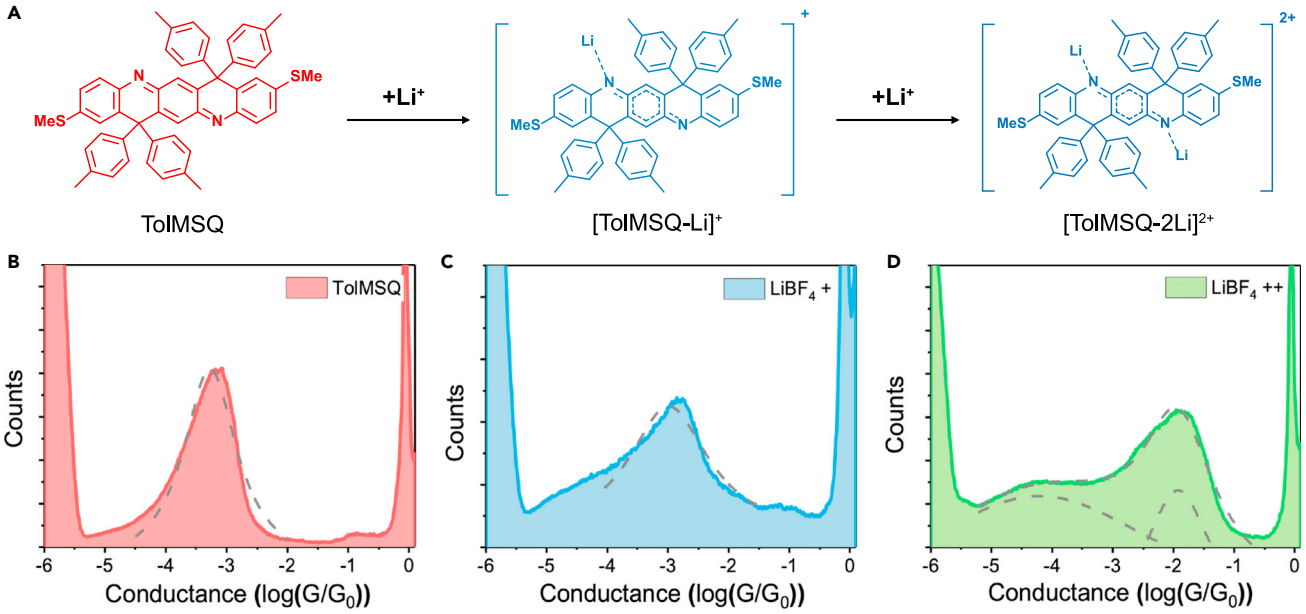

Figure 4. Molecular charge transport in lithiated ladder-type junctions

(A) Chemical structures of lithium coordination with **TolMSQ** molecules.

(B–D) Comparison of the 1D conductance histograms of unlithiated, 50% lithiated, and 100% lithiated **TolMSQ** measured in mixed TCB/THF solvent at 250 mV applied bias. All 1D conductance histograms are compiled from 5,000 to 10,000 individual single molecule measurements and normalized by the total number of measurements without data selection.

such interactions would also be expected to give rise to weak dimerization for neutral **TolMSQ** molecules. However, our single-molecule experiments show no evidence of intermolecular charge transport in the neutral **TolMSQ** state. We therefore hypothesized that the dimerization of charged **[TolMSQ-2H]$^{2+}$** and **[TolMSQ-2Li]$^{2+}$** in single-molecule conductance measurements is promoted by non-covalent radical-radical interactions similar to that observed for viologen radical cations[61–63] and further compensated by counterion-mediated electrostatic interactions. Overall, these results show that molecular conductance can be modulated using Li^+, which broadens the ability to control the molecular conductance of **TolMSQ**, for example by using non-corrosive Li^+ electrolytes via electrochemical control.

Theory and molecular modeling

To understand the role of charge state on molecular conductance in ladder-type conjugated molecules, we used a combination of DFT and nonequilibrium Green's function-DFT (NEGF-DFT) (supplemental information). First, geometry optimization and molecular orbital calculation of neutral **TolMSB**, neutral **TolMSQ**, charged **[TolMSQ-2H]$^{2+}$**, and charged **[TolMSQ-2Li]$^{2+}$** with different multiplicities (singlet and triplet) were performed using the B3LYP functional with a 6-31G(d,p) basis set (Figures 5A and S20). The frontier molecular orbitals show higher orbital weights on terminal –SMe anchor groups in **TolMSQ**, **[TolMSQ-2H]$^{2+}$**, and **[TolMSQ-2Li]$^{2+}$** that enhance coupling with the electrode and result in increased electron transport compared with **TolMSB**.[64] Based on the frontier orbital energies of the four different molecular states (Figure 5B), the estimated band gaps are significantly decreased from the partially conjugated **TolMSB** to fully conjugated **TolMSQ**, with the smallest band gaps observed for **[TolMSQ-2H]$^{2+}$** and **[TolMSQ-2Li]$^{2+}$**. Molecules with relatively small energy band gaps benefit from changes in both the highest occupied molecular orbital (HOMO) and the lowest unoccupied energy molecular orbital (LUMO), assuming that the Fermi energy of the electrodes lies between the molecular HOMO and LUMO energies.[65,66]

Please cite this article in press as: Li et al., Ladder-type conjugated molecules as robust multi-state single-molecule switches, Chem (2023), https://doi.org/10.1016/j.chempr.2023.05.001

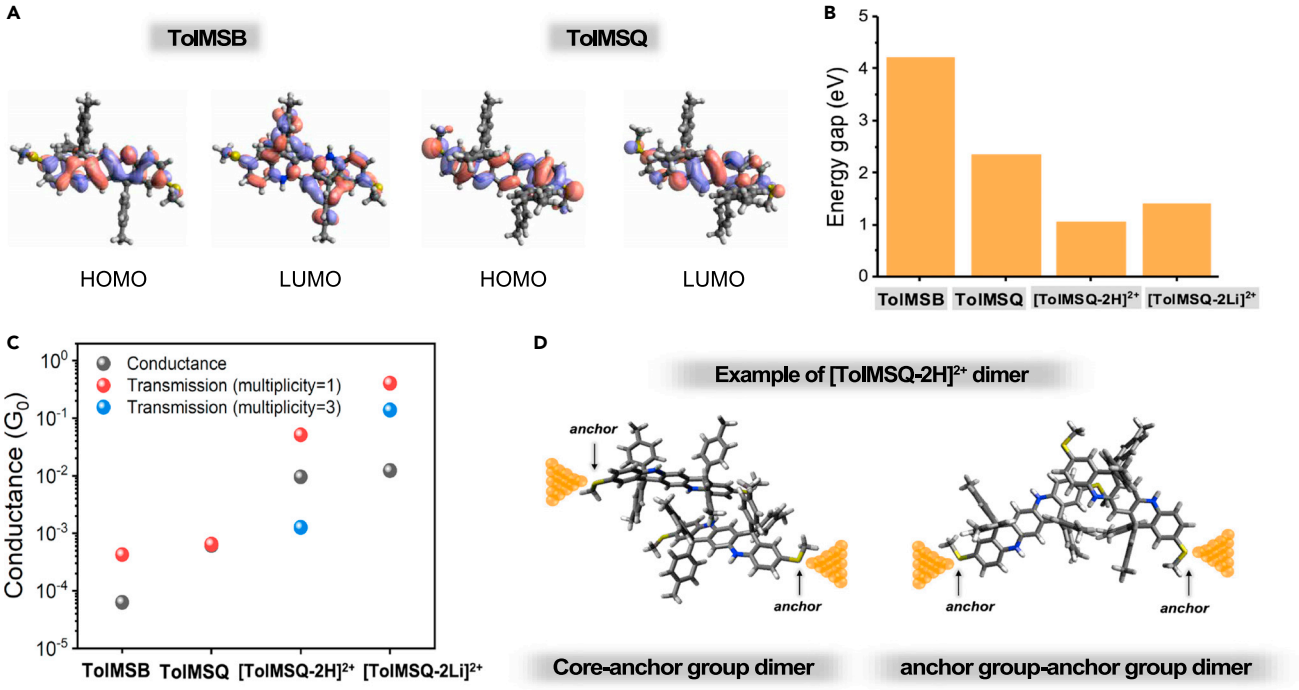

Figure 5. Molecular modeling and DFT simulations of ladder-type molecules

(A) HOMO and LUMO frontier molecular orbitals of **TolMSB** and **TolMSQ**.

(B) Energy gaps in **TolMSQ** species at various molecular states.

(C) Zero-bias transmission of **TolMSB**, **TolMSQ**, **[TolMSQ-2H]$^{2+}$** (singlet and triplet), and **[TolMSQ-2Li]$^{2+}$** (singlet and triplet).

(D) Two types of lowest energy stacked **[TolMSQ-2H]$^{2+}$** dimer configurations determined from DFT geometry optimization. The anchor thiomethyl (–SMe) groups are denoted by arrows.

We next performed transmission calculations using NEGF-DFT simulations (Atomistic Toolkit package) for molecular junctions based on **TolMSB**, **TolMSQ**, **[TolMSQ-2H]$^{2+}$**, and **[TolMSQ-2Li]$^{2+}$** and their corresponding optimized geometries. The singlet and triplet states form resonant structures for **[TolMSQ-2H]$^{2+}$** and **[TolMSQ-2Li]$^{2+}$**; hence, optimized molecular geometries were used with both multiplicities in transmission calculations. To maintain charge neutrality, BF_4^- anions are located in the vicinity of the protonated and lithiated **TolMSQ** in each system. Results from the NEGF-DFT simulations are qualitatively consistent with the overall trends observed in experiments, with the exception of molecular transmission in the triplet state lower than in the singlet state, likely due to the less planar nature of the open-shell triplet state (Figures 5C, S21, and S22). Conjugated molecules with an open-shell triplet structure tend to adopt a less planar conformation and thus the π-electron topologies are disrupted, resulting in a lower calculated transmission compared with the molecules with quinoidal structure.[67,68] Moreover, the optimized geometries of **TolMSQ** under different charge states show that the molecular backbone in the dicationic state (**[TolMSQ-2H]$^{2+}$** and **[TolMSQ-2Li]$^{2+}$**) is less distorted compared with the neutral state (Figure S23), although the ladder-type modification hinders bond rotation in all cases. Enhanced backbone rigidity promotes dimerization in the dicationic state with an unexpected intermolecular conductance level that was not observed in the neutral state molecules **TolMSB** and **TolMSQ**. Overall, experiments and simulation results are consistent with those of prior works, confirming that the open-shell character in conjugated systems enhances molecular charge transport.[69,70]

Please cite this article in press as: Li et al., Ladder-type conjugated molecules as robust multi-state single-molecule switches, Chem (2023), https://doi.org/10.1016/j.chempr.2023.05.001

We further investigated molecular stacked geometries arising in the protonated and lithiated dicationic states using virtual screening workflows. Monomer geometries were first optimized using the GFN2-xTB semiempirical tight-binding model.[71] From the optimized geometries, 10,000 dimer structures were randomly sampled, from which 100 geometries with the lowest energies were selected and further optimized using GFN2-xTB in analytical linearized Poisson-Boltzmann (ALPB) model.[72] Dimers within 20 kJ/mol of the lowest conformation were selected and optimized at the PBE/def2-TZVP level of theory with the D3BJ dispersion correction[73] and a conductor-like polarizable continuum model (CPCM) using ORCA 5.0.[74,75] In general, the dicationic states of protonated or lithiated **TolMSQ** aggregated in two characteristic forms after the geometry optimization calculation: a core-anchor group type dimer where the anchor group overlaps with the molecular backbone and an anchor group-anchor group type dimer where the anchor groups interact with each other (Figures S24 and S25). Similar dimerization behavior has been reported in molecular simulations and crystalline data from experiments with other organic small molecules such as FINIC, ITIC, and Y6.[76–79] Figure 5D shows two representative examples of **[TolMSQ-2H]$^{2+}$** with core-anchor group or anchor group-anchor group geometries at the lowest energy. The distance between two anchors is measured for each type of geometry (core-anchor group: 20.63 Å; anchor group-anchor group: 21.64 Å) and is comparable with the experimentally determined junction lengths after correcting for the junction snap-back distance, as discussed above. Interestingly, **[TolMSQ-2H]$^{2+}$** forms lower energy dimer complexes compared with **[TolMSQ-2Li]$^{2+}$** complexes, possibly due to the less distorted monomer backbone for **[TolMSQ-2H]$^{2+}$**. In addition, the anchor group-anchor group form exists with less steric hindrance and therefore represents the dominant structure in **[TolMSQ-2Li]$^{2+}$** dimers.

We next used NEGF-DFT simulations to determine the transmission of each optimized dimer complex in the presence of counterions (Tables S5 and S6). Reasonable qualitative agreement is observed between experiments and simulations, although precise quantitative agreement between the experimental results is not generally expected due to chemical complexity,[80] electrostatic polarization from the gold electrodes,[81] self-interaction errors in the PBE exchange-correlation functional,[82] and inaccurate electrode Fermi levels using DFT.[83] Nevertheless, the dimer conductance measurement samples a wide range of molecular conformations due to dynamics in the stacked dimer complexes, and multiple molecular geometries are expected to contribute to the outcome. Overall, the simulation results support the increase in molecular conductance from **TolMSB** to **TolMSQ** and are consistent with experiments showing high conductance values in fully protonated and lithiated **TolMSQ**.

Redox state switching using electrochemical control

The reversible redox switching of ladder-type PANI derivatives can also be conducted electrochemically.[36] Here, we demonstrate that the conductance of single **TolMSQ** molecules can also be switched *in situ* using electrochemical modulation (Figure 6A), which can be viewed as the single-molecule analog of bulk-level switching in OECT devices using a gate electrode. For these experiments, the standard STM-BJ experimental setup is modified by adding a platinum electrode as the gate electrode (Figure 6B), as previously described.[84,85] Electrochemical switching of single-molecule junctions is accomplished by applying a gate voltage V_g to the platinum gate electrode (relative to the substrate electrode) in a custom electrochemical cell. Prior to performing single-molecule electrochemical experiments on **TolMSQ**, *in situ* linear sweep voltammetry (LSV) and sweep-rate dependent cyclic

Please cite this article in press as: Li et al., Ladder-type conjugated molecules as robust multi-state single-molecule switches, Chem (2023), https://doi.org/10.1016/j.chempr.2023.05.001

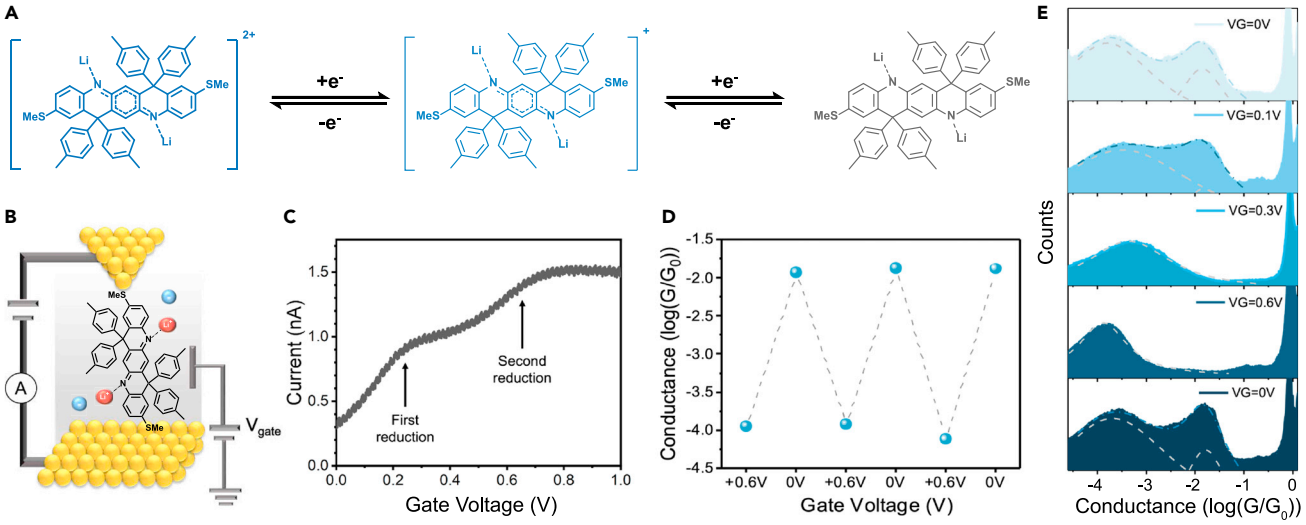

Figure 6. Electrochemical triggered reversible switching of molecular conductance

(A) Chemical structures of the reversible redox-active process of **TolMSQ** with lithium salt coordination.

(B) Schematic of the electrochemical STM-BJ experiment.

(C) *In situ* linear sweep voltammetry (LSV) of **TolMSQ** with $LiBF_4$.

(D) 1D conductance histograms of lithium-ion coordinated **TolMSQ** (1 mM **TolMSQ** with 10 mM $LiBF_4$ in propylene carbonate [PC]) measured at various gate voltages V_g with 100 mV applied bias during the reduction process, each compiled from 5,000 single traces without data selection.

(E) Reversible on-off conductance switches of **TolMSQ-Li** system by electrochemical reduction reoxidation.

voltammetry (CV) were performed by sweeping the gate voltage V_g to determine the potential range of the redox reaction (Figures 6C and S26). Single-molecule conductance experiments are then performed in propylene carbonate (PC) in the presence of lithium salts by varying the gate voltage V_g within the electrochemical window while maintaining a constantly applied bias V_b of 100 mV between the tip and substrate electrode.

Single-molecule electrochemical STM-BJ experiments were performed over a range of gate voltage between V_g = 0 and 0.6 V (Figures 6E and S27). Two conductance peaks were observed in both 1D and 2D histograms at zero-gate voltage. Intermolecular charge transport in the low *G* molecular junction was also confirmed by flicker noise analysis with a normalization factor of 1.6, although the intramolecular charge transport dominated in the high *G* junction with a normalization factor of 1.0 (Figure S28). The low *G* molecular junction only exists in the fully lithiated state, which agrees with the results obtained from the standard STM-BJ setup in TCB/THF solvents without the gate electrode. 1D and 2D molecular conductance histograms maintain the two-peak feature until the gate voltage is increased to V_g = 0.2 V. After the first reduction step, the low *G* peak decreases in magnitude for V_g > 0.2 V, and the remaining conductance peak abruptly shifts to a lower value of around $10^{-3.0}$ G_0. The molecular conductance gradually decreases in the range of $10^{-3.0}$–$10^{-3.3}$ G_0 between gate voltages of V_g = 0.2–0.4 V. As **TolMSQ** was reduced to the benzenoidal structure for V_g > 0.5 V, the molecular conductance sharply drops to $10^{-3.9}$ G_0 and subsequently maintains the same level. Compared with the chemically reduced **TolMSQ**, the electrochemically reduced **TolMSQ** exhibits a slightly higher average conductance due to the presence of lithium coordination. Doping chemically reduced **TolMSQ** with lithium salts in PC reproduced the identical 1D conductance histogram as electrochemical reduction (Figure S29). Finally, on reverting the gate voltage to V_g = 0 V, **TolMSQ** was re-oxidized, and the conductance returns to a high level at $10^{-1.8}$ G_0. Overall, our results show that the ladder-type molecular

Please cite this article in press as: Li et al., Ladder-type conjugated molecules as robust multi-state single-molecule switches, Chem (2023), https://doi.org/10.1016/j.chempr.2023.05.001

system serves as a robust single-molecule switch with a remarkable on/off ratio over two orders of magnitude (≈125×) and is reversible by alternating the gate voltage V_g between 0.6 and 0 V over 500 measurements (Figures 6D and S30).

Conclusions

In this work, we characterize the charge transport properties of a fully conjugated ladder-type molecule at various protonated, lithiated, and redox states using single-molecule experiments and molecular modeling. Our results show that the molecular conductance of the quinoidal molecule **TolMSQ** is 10-fold higher than the reduced form **TolMSB** and can be further enhanced by over an order of magnitude upon full protonation and lithiation to the dicationic state. Intermolecular charge transport is observed via the formation of a stacked dimer. We further demonstrate an *in situ* molecular conductance switch using electrochemical potential to induce redox reactions in lithium salt environments, resulting in a single-molecule switch with an on/off ratio of ≈125. Experimental results are complemented by molecular modeling and DFT simulations, which provide insight into the molecular charge transport pathways for different charge states of **TolMSQ**. A core-anchor group type and anchor group-anchor group type of dimer geometries are observed from DFT simulations, which reveal the intermolecular charge transport pathways in stacked **TolMSQ** molecules.

Overall, these results demonstrate that ladder-type conjugated molecules provide a promising class of materials for the application of functional molecular electronics with remarkable electronic properties and stability. Electrochemical STM-BJ experiments further prove the fundamental concept of a multi-state single molecule OECT and provide mechanistic insight into the electrochemical transistor behavior of the ladder-type oligoaniline at the single-molecule level. Stable multi-state conductivity switching in this type of material can be achieved by protonation, lithium-ion coordination, and redox reaction. Furthermore, we believe that increasing aniline units in longer ladder-type molecules can not only maintain its high conductance level due to the structural rigidity but also enable the access to a larger number of stable conductance states, which are both critical to the device application of OECT. Future work will focus on the synthesis of long molecular wires, in addition to molecular design considerations such as side-chain optimization, to exploit the doping chemistry and metallic conductivity conjugated ladder-type PANI derivatives.

EXPERIMENTAL PROCEDURES

Resource availability

Lead contact

Further information and requests for resources should be directed to and will be fulfilled by the lead contact Charles M. Schroeder (cms@illinois.edu).

Materials availability

This study did not generate new unique reagents.

Data and code availability

All data needed to support the conclusions of this manuscript are included in the main text or the supplemental information.

SUPPLEMENTAL INFORMATION

Supplemental information can be found online at https://doi.org/10.1016/j.chempr.2023.05.001.

ACKNOWLEDGMENTS

The research was financially supported by the Joint Center for Energy Storage Research (JCESR), an Energy Innovation Hub funded by the U.S. Department of Energy, Office of Science, Basic Energy Sciences, the President's X-Grants Initiative at Texas A&M University, and the Robert A. Welch Foundation (A-1898). D.P.T. and S.L. acknowledge support from Texas A&M Department of Chemistry startup funds and the Robert A. Welch Foundation (A-2049). Portions of this research were conducted with the advanced computing resources provided by Texas A&M High Performance Research Computing.

AUTHOR CONTRIBUTIONS

J.L., B.-J.P., L.F., and C.M.S. conceptualized the project and designed the studies. J.L. performed single-molecule experiments. B.-J.P. performed synthesis and chemical characterization on the molecules. S.L. and J.L. performed DFT and NEGF-DFT calculations. Data were curated and formally analyzed by J.L. and B.-J.P. The manuscript was written through contributions of all authors. The project was supervised by D.P.T., L.F., and C.M.S. Funding was acquired by D.P.T., L.F., and C.M.S.

DECLARATION OF INTERESTS

The authors declare no competing interests.

Received: January 3, 2023
Revised: March 25, 2023
Accepted: April 17, 2023
Published: May 24, 2023

REFERENCES

1. Aviram, A., and Ratner, M.A. (1974). Molecular rectifiers. Chem. Phys. Lett. *29*, 277–283. https://doi.org/10.1016/0009-2614(74)85031-1.

2. Puebla-Hellmann, G., Venkatesan, K., Mayor, M., and Lörtscher, E. (2018). Metallic nanoparticle contacts for high-yield, ambient-stable molecular-monolayer devices. Nature *559*, 232–235. https://doi.org/10.1038/s41586-018-0275-z.

3. Aradhya, S.V., and Venkataraman, L. (2013). Single-molecule junctions beyond electronic transport. Nat. Nanotechnol. *8*, 399–410. https://doi.org/10.1038/nnano.2013.91.

4. Chen, H., and Fraser Stoddart, J. (2021). From molecular to supramolecular electronics. Nat. Rev. Mater. *6*, 804–828. https://doi.org/10.1038/s41578-021-00302-2.

5. Zhang, J.L., Zhong, J.Q., Lin, J.D., Hu, W.P., Wu, K., Xu, G.Q., Wee, A.T., and Chen, W. (2015). Towards single molecule switches. Chem. Soc. Rev. *44*, 2998–3022. https://doi.org/10.1039/c4cs00377b.

6. Li, Z., Smeu, M., Afsari, S., Xing, Y., Ratner, M.A., and Borguet, E. (2014). Single-molecule sensing of environmental pH–an STM break junction and NEGF-DFT approach. Angew. Chem. Int. Ed. Engl. *53*, 1098–1102. https://doi.org/10.1002/anie.201308398.

7. Jia, C., Migliore, A., Xin, N., Huang, S., Wang, J., Yang, Q., Wang, S., Chen, H., Wang, D., Feng, B., et al. (2016). Covalently bonded single-molecule junctions with stable and reversible photoswitched conductivity. Science *352*, 1443–1445. https://doi.org/10.1126/science.aaf6298.

8. Han, Y., Nickle, C., Zhang, Z., Astier, H.P.A.G., Duffin, T.J., Qi, D., Wang, Z., Del Barco, E., Thompson, D., and Nijhuis, C.A. (2020). Electric-field-driven dual-functional molecular switches in tunnel junctions. Nat. Mater. *19*, 843–848. https://doi.org/10.1038/s41563-020-0697-5.

9. Aragonès, A.C., Aravena, D., Cerdá, J.I., Acís-Castillo, Z., Li, H., Real, J.A., Sanz, F., Hihath, J., Ruiz, E., and Díez-Pérez, I. (2016). Large conductance switching in a single-molecule device through room temperature spin-dependent transport. Nano Lett. *16*, 218–226. https://doi.org/10.1021/acs.nanolett.5b03571.

10. Walkey, M.C., Peiris, C.R., Ciampi, S., C Aragonès, A., Domínguez-Espíndola, R.B., Jago, D., Pulbrook, T., Skelton, B.W., Sobolev, A.N., Díez Pérez, I., et al. (2019). Chemically and mechanically controlled single-molecule switches using spiropyrans. ACS Appl. Mater. Interfaces *11*, 36886–36894. https://doi.org/10.1021/acsami.9b11044.

11. Baghernejad, M., Zhao, X., Baruël Ørnsø, K., Füeg, M., Moreno-García, P., Rudnev, A.V., Kaliginedi, V., Vesztergom, S., Huang, C., Hong, W., et al. (2014). Electrochemical control of single-molecule conductance by Fermi-level tuning and conjugation switching. J. Am. Chem. Soc. *136*, 17922–17925. https://doi.org/10.1021/ja510335z.

12. Chen, H., Jiang, F., Hu, C., Jiao, Y., Chen, S., Qiu, Y., Zhou, P., Zhang, L., Cai, K., Song, B., et al. (2021). Electron-catalyzed dehydrogenation in a single-molecule junction. J. Am. Chem. Soc. *143*, 8476–8487. https://doi.org/10.1021/jacs.1c03141.

13. Ward, J.S., and Vezzoli, A. (2022). Key advances in electrochemically-addressable single-molecule electronics. Curr. Opin. Electrochem. *35*. https://doi.org/10.1016/j.coelec.2022.101083.

14. Pappa, A.M., Ohayon, D., Giovannitti, A., Maria, I.P., Savva, A., Uguz, I., Rivnay, J., McCulloch, I., Owens, R.M., and Inal, S. (2018). Direct metabolite detection with an n-type accumulation mode organic electrochemical transistor. Sci. Adv. *4*, eaat0911. https://doi.org/10.1126/sciadv.aat0911.

15. Han, S., Yamamoto, S., Polyravas, A.G., and Malliaras, G.G. (2020). Microfabricated ion-selective transistors with fast and super-Nernstian response. Adv. Mater. *32*, e2004790. https://doi.org/10.1002/adma.202004790.

16. Williamson, A., Ferro, M., Leleux, P., Ismailova, E., Kaszas, A., Doublet, T., Quilichini, P., Rivnay, J., Rózsa, B., Katona, G., et al. (2015). Localized neuron stimulation with organic electrochemical transistors on delaminating depth probes. Adv. Mater. *27*, 4405–4410. https://doi.org/10.1002/adma.201500218.

17. Ji, X., Paulsen, B.D., Chik, G.K.K., Wu, R., Yin, Y., Chan, P.K.L., and Rivnay, J. (2021). Mimicking

associative learning using an ion-trapping non-volatile synaptic organic electrochemical transistor. Nat. Commun. *12*, 2480. https://doi.org/10.1038/s41467-021-22680-5.

18. Hidalgo Castillo, T.C., Moser, M., Cendra, C., Nayak, P.D., Salleo, A., McCulloch, I., and Inal, S. (2022). Simultaneous performance and stability improvement of a p-type organic electrochemical transistor through additives. Chem. Mater. *34*, 6723–6733. https://doi.org/10.1021/acs.chemmater.2c00632.

19. Griggs, S., Marks, A., Bristow, H., and McCulloch, I. (2021). n-type organic semiconducting polymers: stability limitations, design considerations and applications. J. Mater. Chem. C Mater. *9*, 8099–8128. https://doi.org/10.1039/d1tc02048j.

20. Rivnay, J., Inal, S., Salleo, A., Owens, R.M., Berggren, M., and Malliaras, G.G. (2018). Organic electrochemical transistors. Nat. Rev. Mater. *3*, 17086. https://doi.org/10.1038/natrevmats.2017.86.

21. Inal, S., Malliaras, G.G., and Rivnay, J. (2017). Benchmarking organic mixed conductors for transistors. Nat. Commun. *8*, 1767. https://doi.org/10.1038/s41467-017-01812-w.

22. Mabeck, J.T., and Malliaras, G.G. (2006). Chemical and biological sensors based on organic thin-film transistors. Anal. Bioanal. Chem. *384*, 343–353. https://doi.org/10.1007/s00216-005-3390-2.

23. Jiménez, P., Levillain, E., Alévêque, O., Guyomard, D., Lestriez, B., and Gaubicher, J. (2017). Lithium n-doped polyaniline as a high-performance electroactive material for rechargeable batteries. Angew. Chem. Int. Ed. Engl. *56*, 1553–1556. https://doi.org/10.1002/anie.201607820.

24. Ji, X., Xie, H., Zhu, C., Zou, Y., Mu, A.U., Al-Hashimi, M., Dunbar, K.R., and Fang, L. (2020). Pauli paramagnetism of stable analogues of pernigraniline salt featuring ladder-type constitution. J. Am. Chem. Soc. *142*, 641–648. https://doi.org/10.1021/jacs.9b12626.

25. Li, S., Jira, E.R., Angello, N.H., Li, J., Yu, H., Moore, J.S., Diao, Y., Burke, M.D., and Schroeder, C.M. (2022). Using automated synthesis to understand the role of side chains on molecular charge transport. Nat. Commun. *13*, 2102. https://doi.org/10.1038/s41467-022-29796-2.

26. Venkataraman, L., Klare, J.E., Nuckolls, C., Hybertsen, M.S., and Steigerwald, M.L. (2006). Dependence of single-molecule junction conductance on molecular conformation. Nature *442*, 904–907. https://doi.org/10.1038/nature05037.

27. Mishchenko, A., Vonlanthen, D., Meded, V., Bürkle, M., Li, C., Pobelov, I.V., Bagrets, A., Viljas, J.K., Pauly, F., Evers, F., et al. (2010). Influence of conformation on conductance of biphenyl-dithiol single-molecule contacts. Nano Lett. *10*, 156–163. https://doi.org/10.1021/nl903084b.

28. Capozzi, B., Dell, E.J., Berkelbach, T.C., Reichman, D.R., Venkataraman, L., and Campos, L.M. (2014). Length-dependent conductance of oligothiophenes. J. Am. Chem. Soc. *136*, 10486–10492. https://doi.org/10.1021/ja505277z.

29. Lee, W., Louie, S., Evans, A.M., Orchanian, N.M., Stone, I.B., Zhang, B., Wei, Y., Roy, X., Nuckolls, C., and Venkataraman, L. (2022). Increased molecular conductance in oligo[n]phenylene wires by thermally enhanced dihedral planarization. Nano Lett. *22*, 4919–4924. https://doi.org/10.1021/acs.nanolett.2c01549.

30. Tang, Y., Zhou, Y., Zhou, D., Chen, Y., Xiao, Z., Shi, J., Liu, J., and Hong, W. (2020). Electric field-induced assembly in single-stacking terphenyl junctions. J. Am. Chem. Soc. *142*, 19101–19109. https://doi.org/10.1021/jacs.0c07348.

31. Li, J., Pudar, S., Yu, H., Li, S., Moore, J.S., Rodríguez-López, J., Jackson, N.E., and Schroeder, C.M. (2021). Reversible switching of molecular conductance in viologens is controlled by the electrochemical environment. J. Phys. Chem. C *125*, 21862–21872. https://doi.org/10.1021/acs.jpcc.1c06942.

32. Lee, J., Kalin, A.J., Yuan, T., Al-Hashimi, M., and Fang, L. (2017). Fully conjugated ladder polymers. Chem. Sci. *8*, 2503–2521. https://doi.org/10.1039/c7sc00154a.

33. Cai, Z., Awais, M.A., Zhang, N., and Yu, L. (2018). Exploration of syntheses and functions of higher ladder-type π-conjugated heteroacenes. Chem *4*, 2538–2570. https://doi.org/10.1016/j.chempr.2018.08.017.

34. Cai, Z., Lo, W.Y., Zheng, T., Li, L., Zhang, N., Hu, Y., and Yu, L. (2016). Exceptional single-molecule transport properties of ladder-type heteroacene molecular wires. J. Am. Chem. Soc. *138*, 10630–10635. https://doi.org/10.1021/jacs.6b05983.

35. Zhu, C., Kalin, A.J., and Fang, L. (2019). Covalent and noncovalent approaches to rigid coplanar pi-conjugated molecules and macromolecules. Acc. Chem. Res. *52*, 1089–1100. https://doi.org/10.1021/acs.accounts.9b00022.

36. Ji, X., Leng, M., Xie, H., Wang, C., Dunbar, K.R., Zou, Y., and Fang, L. (2020). Extraordinary electrochemical stability and extended polaron delocalization of ladder-type polyaniline-analogous polymers. Chem. Sci. *11*, 12737–12745. https://doi.org/10.1039/d0sc03348k.

37. Moon, D.-K., Ezuka, M., Maruyama, T., Osakada, K., and Yamamoto, T. (1993). Chemical reduction of the emeraldine base of polyaniline by reducing agents and its kinetic study. Makromol. Chem. *194*, 3149–3155. https://doi.org/10.1002/macp.1993.021941118.

38. Makarov, S.V., Kudrik, E.V., van Eldik, R., and Naidenko, E.V. (2002). Reactions of methyl viologen and nitrite with thiourea dioxide. New opportunities for an old reductant. J. Chem. Soc. Dalton Trans. 4074–4076. https://doi.org/10.1039/b209195j.

39. Yu, H., Li, S., Schwieter, K.E., Liu, Y., Sun, B., Moore, J.S., and Schroeder, C.M. (2020). Charge transport in sequence-defined conjugated oligomers. J. Am. Chem. Soc. *142*, 4852–4861. https://doi.org/10.1021/jacs.0c00043.

40. Li, S., Li, J., Yu, H., Pudar, S., Li, B., Rodríguez-López, J., Moore, J.S., and Schroeder, C.M. (2020). Characterizing intermolecular interactions in redox-active pyridinium-based molecular junctions. J. Electroanal. Chem *875*. https://doi.org/10.1016/j.jelechem.2020.114070.

41. Li, B., Yu, H., Montoto, E.C., Liu, Y., Li, S., Schwieter, K., Rodríguez-López, J., Moore, J.S., and Schroeder, C.M. (2019). Intrachain charge transport through conjugated donor–acceptor oligomers. ACS Appl. Electron. Mater. *1*, 7–12. https://doi.org/10.1021/acsaelm.8b00050.

42. Moreno-García, P., Gulcur, M., Manrique, D.Z., Pope, T., Hong, W., Kaliginedi, V., Huang, C., Batsanov, A.S., Bryce, M.R., Lambert, C., et al. (2013). Single-molecule conductance of functionalized oligoynes: length dependence and junction evolution. J. Am. Chem. Soc. *135*, 12228–12240. https://doi.org/10.1021/ja4015293.

43. Gao, T., Pan, Z., Cai, Z., Zheng, J., Tang, C., Yuan, S., Zhao, S.Q., Bai, H., Yang, Y., Shi, J., et al. (2021). Electric field-induced switching among multiple conductance pathways in single-molecule junctions. Chem. Commun. (Camb) *57*, 7160–7163. https://doi.org/10.1039/d1cc02111g.

44. Bogomolova, O.E., and Sergeyev, V.G. (2018). Acid doping of phenyl-capped aniline dimer: intermolecular polaron formation mechanism and its applicability to polyaniline. J. Phys. Chem. A *122*, 461–469. https://doi.org/10.1021/acs.jpca.7b09851.

45. Boeva, Z.A., and Sergeyev, V.G. (2014). Polyaniline: synthesis, properties, and application. Polym. Sci. Ser. C *56*, 144–153. https://doi.org/10.1134/S1811238214010032.

46. Baird, N.C. (1972). Quantum organic photochemistry. II. Resonance and aromaticity in the lowest 3.pi..pi.* state of cyclic hydrocarbons. J. Am. Chem. Soc. *94*, 4941–4948. https://doi.org/10.1021/ja00769a025.

47. Lin, L., Tang, C., Dong, G., Chen, Z., Pan, Z., Liu, J., Yang, Y., Shi, J., Ji, R., and Hong, W. (2021). Spectral clustering to analyze the hidden events in single-molecule break junctions. J. Phys. Chem. C *125*, 3623–3630. https://doi.org/10.1021/acs.jpcc.0c11473.

48. Feng, A., Zhou, Y., Al-Shebami, M.A.Y., Chen, L., Pan, Z., Xu, W., Zhao, S., Zeng, B., Xiao, Z., Yang, Y., et al. (2022). σ–σ Stacked supramolecular junctions. Nat. Chem. *14*, 1158–1164. https://doi.org/10.1038/s41557-022-01003-1.

49. Magyarkuti, A., Adak, O., Halbritter, A., and Venkataraman, L. (2018). Electronic and mechanical characteristics of stacked dimer molecular junctions. Nanoscale *10*, 3362–3368. https://doi.org/10.1039/c7nr08354h.

50. Makk, P., Tomaszewski, D., Martinek, J., Balogh, Z., Csonka, S., Wawrzyniak, M., Frei, M., Venkataraman, L., and Halbritter, A. (2012). Correlation analysis of atomic and single-molecule junction conductance. ACS Nano *6*, 3411–3423. https://doi.org/10.1021/nn300440f.

51. Huang, C., Jevric, M., Borges, A., Olsen, S.T., Hamill, J.M., Zheng, J.T., Yang, Y., Rudnev, A., Baghernejad, M., Broekmann, P., et al. (2017). Single-molecule detection of dihydroazulene photo-thermal reaction using break junction

technique. Nat. Commun. *8*. 15436. https://doi.org/10.1038/ncomms15436.

52. Mishchenko, A., Zotti, L.A., Vonlanthen, D., Bürkle, M., Pauly, F., Cuevas, J.C., Mayor, M., and Wandlowski, T. (2011). Single-molecule junctions based on nitrile-terminated biphenyls: a promising new anchoring group. J. Am. Chem. Soc. *133*, 184–187. https://doi.org/10.1021/ja107340t.

53. Adak, O., Rosenthal, E., Meisner, J., Andrade, E.F., Pasupathy, A.N., Nuckolls, C., Hybertsen, M.S., and Venkataraman, L. (2015). Flicker noise as a probe of electronic interaction at metal-single molecule interfaces. Nano Lett. *15*, 4143–4149. https://doi.org/10.1021/acs.nanolett.5b01270.

54. Li, X., Wu, Q., Bai, J., Hou, S., Jiang, W., Tang, C., Song, H., Huang, X., Zheng, J., Yang, Y., et al. (2020). Structure-independent conductance of thiophene-based single-stacking junctions. Angew. Chem. Int. Ed. Engl. *59*, 3280–3286. https://doi.org/10.1002/anie.201913344.

55. Fu, T., Smith, S., Camarasa-Gómez, M., Yu, X., Xue, J., Nuckolls, C., Evers, F., Venkataraman, L., and Wei, S. (2019). Enhanced coupling through pi-stacking in imidazole-based molecular junctions. Chem. Sci. *10*, 9998–10002. https://doi.org/10.1039/c9sc03760h.

56. Tang, C., Tang, Y., Ye, Y., Yan, Z., Chen, Z., Chen, L., Zhang, L., Liu, J., Shi, J., Xia, H., et al. (2020). Identifying the conformational isomers of single-molecule cyclohexane at room temperature. Chem *6*, 2770–2781. https://doi.org/10.1016/j.chempr.2020.07.024.

57. Hollingsworth, W.R., Lee, J., Fang, L., and Ayzner, A.L. (2017). Exciton relaxation in highly rigid conjugated polymers: correlating radiative dynamics with structural heterogeneity and wavefunction delocalization. ACS Energy Lett. *2*, 2096–2102. https://doi.org/10.1021/acsenergylett.7b00535.

58. Zhu, C., Guo, Z.H., Mu, A.U., Liu, Y., Wheeler, S.E., and Fang, L. (2016). Low band gap coplanar conjugated molecules featuring dynamic intramolecular lewis acid-base coordination. J. Org. Chem. *81*, 4347–4352. https://doi.org/10.1021/acs.joc.6b00238.

59. Cai, Z., Zhang, N., Awais, M.A., Filatov, A.S., and Yu, L. (2018). Synthesis of alternating donor-acceptor ladder-type molecules and investigation of their multiple charge-transfer pathways. Angew. Chem. Int. Ed. Engl. *57*, 6442–6448. https://doi.org/10.1002/anie.201713323.

60. Yu, H., Li, J., Li, S., Liu, Y., Jackson, N.E., Moore, J.S., and Schroeder, C.M. (2022). Efficient intermolecular charge transport in pi-stacked pyridinium dimers using cucurbit[8]uril supramolecular complexes. J. Am. Chem. Soc. *144*, 3162–3173. https://doi.org/10.1021/jacs.1c12741.

61. Geraskina, M.R., Dutton, A.S., Juetten, M.J., Wood, S.A., and Winter, A.H. (2017). The viologen cation radical pimer: a case of dispersion-driven bonding. Angew. Chem. Int. Ed. Engl. *56*, 9435–9439. https://doi.org/10.1002/anie.201704959.

62. Trabolsi, A., Khashab, N., Fahrenbach, A.C., Friedman, D.C., Colvin, M.T., Cotí, K.K., Benítez, D., Tkatchouk, E., Olsen, J.C., Belowich, M.E., et al. (2010). Radically enhanced molecular recognition. Nat. Chem. *2*, 42–49. https://doi.org/10.1038/nchem.479.

63. Kosower, E.M., and Cotter, J.L. (1964). Stable free radicals. II. The reduction of 1-methyl-4-cyanopyridinium ion to methylviologen cation radical. J. Am. Chem. Soc. *86*, 5524–5527. https://doi.org/10.1021/ja01078a026.

64. Reznikova, K., Hsu, C., Schosser, W.M., Gallego, A., Beltako, K., Pauly, F., van der Zant, H.S.J., and Mayor, M. (2021). Substitution pattern controlled quantum interference in [2.2]paracyclophane-based single-molecule junctions. J. Am. Chem. Soc. *143*, 13944–13951. https://doi.org/10.1021/jacs.1c06966.

65. Duan, P., Qu, K., Wang, J.-Y., Zeng, B., Tang, C., Su, H.-F., Zhang, Q.-C., Hong, W., and Chen, Z.-N. (2021). Effective suppression of conductance in multichannel molecular wires. Cell Rep. Phys. Sci. *2*. https://doi.org/10.1016/j.xcrp.2021.100342.

66. Lambert, C.J., and Liu, S.X. (2018). A magic ratio rule for beginners: A chemist's guide to quantum interference in molecules. Chemistry *24*, 4193–4201. https://doi.org/10.1002/chem.201704488.

67. Yuan, B., Li, C., Zhao, Y., Gröning, O., Zhou, X., Zhang, P., Guan, D., Li, Y., Zheng, H., Liu, C., et al. (2020). Resolving quinoid structure in poly(para-phenylene) chains. J. Am. Chem. Soc. *142*, 10034–10041. https://doi.org/10.1021/jacs.0c01930.

68. Casado, J. (2017). Para-quinodimethanes: a unified review of the quinoidal-versus-aromatic competition and its implications. Top. Curr. Chem. (Cham) *375*, 73. https://doi.org/10.1007/s41061-017-0163-2.

69. Li, L., Low, J.Z., Wilhelm, J., Liao, G., Gunasekaran, S., Prindle, C.R., Starr, R.L., Golze, D., Nuckolls, C., Steigerwald, M.L., et al. (2022). Highly conducting single-molecule topological insulators based on mono- and di-radical cations. Nat. Chem. *14*, 1061–1067. https://doi.org/10.1038/s41557-022-00978-1.

70. Naghibi, S., Sangtarash, S., Kumar, V.J., Wu, J.Z., Judd, M.M., Qiao, X., Gorenskaia, E., Higgins, S.J., Cox, N., Nichols, R.J., et al. (2022). Redox-addressable single-molecule junctions incorporating a persistent organic radical. Angew. Chem. Int. Ed. Engl. *61*, e202116985. https://doi.org/10.1002/anie.202116985.

71. Bannwarth, C., Ehlert, S., and Grimme, S. (2019). GFN2-xTB-an accurate and broadly parametrized self-consistent tight-binding quantum chemical method with multipole electrostatics and density-dependent dispersion contributions. J. Chem. Theory Comput. *15*, 1652–1671. https://doi.org/10.1021/acs.jctc.8b01176.

72. Rice, R.E., and Horne, F.H. (1981). Analytical solution of the linearized Poisson–Boltzmann equation in cylindrical coordinates. J. Chem. Phys. *75*, 5582–5583. https://doi.org/10.1063/1.441936.

73. Grimme, S., Ehrlich, S., and Goerigk, L. (2011). Effect of the damping function in dispersion corrected density functional theory. J. Comput. Chem. *32*, 1456–1465. https://doi.org/10.1002/jcc.21759.

74. Neese, F. (2012). The ORCA program system. WIREs Comput. Mol. Sci. *2*, 73–78.

75. Neese, F. (2017). Software update: the ORCA program system, version 4.0. WIREs Comput. Mol. Sci. *8*, e1327.

76. Qin, S., Meng, L., and Li, Y. (2021). Molecular properties and aggregation behavior of small-molecule acceptors calculated by molecular simulation. ACS Omega *6*, 14467–14475. https://doi.org/10.1021/acsomega.1c01394.

77. Dai, S., Zhou, J., Chandrabose, S., Shi, Y., Han, G., Chen, K., Xin, J., Liu, K., Chen, Z., Xie, Z., et al. (2020). High-performance fluorinated fused-ring electron acceptor with 3D stacking and exciton/charge transport. Adv. Mater. *32*, e2000645. https://doi.org/10.1002/adma.202000645.

78. Lin, Y., Wang, J., Zhang, Z.G., Bai, H., Li, Y., Zhu, D., and Zhan, X. (2015). An electron acceptor challenging fullerenes for efficient polymer solar cells. Adv. Mater. *27*, 1170–1174. https://doi.org/10.1002/adma.201404317.

79. Yuan, J., Zhang, Y., Zhou, L., Zhang, G., Yip, H.-L., Lau, T.-K., Lu, X., Zhu, C., Peng, H., Johnson, P.A., et al. (2019). Single-junction organic solar cell with over 15% efficiency using fused-ring acceptor with electron-deficient core. Joule *3*, 1140–1151. https://doi.org/10.1016/j.joule.2019.01.004.

80. Strange, M., Kristensen, I.S., Thygesen, K.S., and Jacobsen, K.W. (2008). Benchmark density functional theory calculations for nanoscale conductance. J. Chem. Phys. *128*, 114714. https://doi.org/10.1063/1.2839275.

81. Neaton, J.B., Hybertsen, M.S., and Louie, S.G. (2006). Renormalization of molecular electronic levels at metal-molecule interfaces. Phys. Rev. Lett. *97*, 216405. https://doi.org/10.1103/PhysRevLett.97.216405.

82. Mowbray, D.J., Jones, G., and Thygesen, K.S. (2008). Influence of functional groups on charge transport in molecular junctions. J. Chem. Phys. *128*, 111103. https://doi.org/10.1063/1.2894544.

83. Lambert, C.J. (2015). Basic concepts of quantum interference and electron transport in single-molecule electronics. Chem. Soc. Rev. *44*, 875–888. https://doi.org/10.1039/c4cs00203b.

84. Capozzi, B., Chen, Q., Darancet, P., Kotiuga, M., Buzzeo, M., Neaton, J.B., Nuckolls, C., and Venkataraman, L. (2014). Tunable charge transport in single-molecule junctions via electrolytic gating. Nano Lett. *14*, 1400–1404. https://doi.org/10.1021/nl404459q.

85. Yin, X., Zang, Y., Zhu, L., Low, J.Z., Liu, Z.F., Cui, J., Neaton, J.B., Venkataraman, L., and Campos, L.M. (2017). A reversible single-molecule switch based on activated antiaromaticity. Sci. Adv. *3*, eaao2615. https://doi.org/10.1126/sciadv.aao2615.